Vacancy-type defects in Al_2O_3/GaN structure probed by monoenergetic positron beams

Akira Uedono, Toshihide Nabatame, Werner Egger, Tönjes Koschine, Christoph Hugenschmidt, Marcel Dickmann, Masatomo Sumiya, and Shoji Ishibashi

Citation: Journal of Applied Physics **123**, 155302 (2018); doi: 10.1063/1.5026831
View online: https://doi.org/10.1063/1.5026831
View Table of Contents: http://aip.scitation.org/toc/jap/123/15
Published by the American Institute of Physics

Vacancy-type defects in Al_2O_3/GaN structure probed by monoenergetic positron beams

Akira Uedono,[1] Toshihide Nabatame,[2] Werner Egger,[3] Tönjes Koschine,[3] Christoph Hugenschmidt,[4] Marcel Dickmann,[4] Masatomo Sumiya,[2] and Shoji Ishibashi[5]
[1]*Division of Applied Physics, Faculty of Pure and Applied Science, University of Tsukuba, Tsukuba, Ibaraki 305-8573, Japan*
[2]*National Institute for Materials Science (NIMS), Tsukuba, Ibaraki 305-0044, Japan*
[3]*Universität der Bundeswehr München, Institut für Angewandte Physik und Messtechnik, 85577 Neubiberg, Germany*
[4]*Physics Department E21 and Heinz Maier-Leibnitz Zentrum (MLZ), Technische Universität München, 85748 Garching, Germany*
[5]*Research Center for Computational Design of Advanced Functional Materials (CD-FMat), National Institute of Advanced Industrial Science and Technology (AIST), Tsukuba, Ibaraki 305-8568, Japan*

(Received 24 February 2018; accepted 30 March 2018; published online 17 April 2018)

Defects in the Al_2O_3(25 nm)/GaN structure were probed by using monoenergetic positron beams. Al_2O_3 films were deposited on GaN by atomic layer deposition at 300 °C. Temperature treatment above 800 °C leads to the introduction of vacancy-type defects in GaN due to outdiffusion of atoms from GaN into Al_2O_3. The width of the damaged region was determined to be 40–50 nm from the Al_2O_3/GaN interface, and some of the vacancies were identified to act as electron trapping centers. In the Al_2O_3 film before and after annealing treatment at 300–900 °C, open spaces with three different sizes were found to coexist. The density of medium-sized open spaces started to decrease above 800 °C, which was associated with the interaction between GaN and Al_2O_3. Effects of the electron trapping/detrapping processes of interface states on the flat band voltage and the defects in GaN were also discussed. *Published by AIP Publishing.* https://doi.org/10.1063/1.5026831

I. INTRODUCTION

Gallium nitride (GaN) and its related alloys [(AlInGa)N] are ideal semiconductors for high-power and high-speed electronics because of their beneficial physical properties, such as a wide bandgap, high saturation electron velocity, sufficient thermal conductivity, and high breakdown voltage.[1,2] GaN-based metal-semiconductor field-effect transistors (MESFETs), therefore, have been extensively studied as next-generation power devices.[3–5] The application and performance of GaN-MESFET, however, were restricted because of their relatively large gate leakage current through the Schottky contact and their normally on operation mode. To suppress the leakage, metal-oxide-semiconductor (MOS) gate stacks for GaN-based devices have been studied extensively. However, compared to Si- and SiC-based MOS devices, forming uniform thin thermal oxides on GaN is difficult. In addition, Ga_2O_3 is not suitable as an insulator because of its insufficient band offsets for GaN.[6–9] Thus, techniques for depositing oxide or nitride films on GaN and their electrical properties have been extensively studied.[10–20] Among many candidates, Al_2O_3 prepared using atomic layer deposition (ALD) is seen as an attractive candidate for GaN-based MOS devices because of its high conduction-band offset on GaN, high dielectric constant, and high breakdown field.

The deposition of gate oxides tends to introduce high-density carrier traps at the interface, and they are the major obstacles in device fabrication. For widegap semiconductors, the energy levels of those traps could be located far from valence or conduction bands exhibiting long-time constants for charge emission at room temperature. This could be an origin for the degradation of the device reliability, such as threshold voltage (V_{th}) instability. For high-k films deposited by ALD for Si-based MOSFET, post-deposition annealing is usually done at around 1000 °C to improve the quality of the films and high-k/Si interfaces.[21] Compared to Si or SiC, because the interfacial reaction of the insulator and GaN could occur easily, the post-deposition annealing temperature should be kept as low as possible. Here, the reaction involves not only chemical reactions between oxides and GaN, but also the mass exchange between insulators and semiconductors. Thus, knowledge on the interface reaction between oxides and GaN is a key to developing GaN-based MOS devices. Positron annihilation is a useful technique for characterizing vacancy-type defects in semiconductors,[22,23] and it has been successfully used to detect defects in GaN.[24–27] This technique is also useful for detecting open spaces in thin amorphous films deposited on semiconductor substrates.[28,29] In the present study, we used monoenergetic positron beams to study reactions between ALD-Al_2O_3 and GaN during post-deposition annealing and annealing behaviors of open spaces in ALD-Al_2O_3.

II. EXPERIMENT

The GaN templates used in this study were 5-μm-thick Si-doped GaN grown on c+-GaN substrates by metal-organic vapor phase deposition. Top GaN layers with a Si concentration of 2×10^{16} cm^{-3} were grown by hydride vapor phase epitaxy (HVPE). The density of the threading dislocations of the templates was estimated to be lower than 10^7 cm^{-2} by wet etching. Before depositing ALD-Al_2O_3, the templates

were treated with a sulfuric acid peroxide mixture (H_2SO_4:H_2O_2 = 1:1). Using low-energy ion scattering spectroscopy, it was found that this treatment formed a sub-nm-thick GaO_x layer (native oxide) on the template surface,[30] and 25-nm-thick Al_2O_3 films were deposited on the template by using the ALD method. Trimethylaluminium [TMA: $Al(CH_3)_3$] and H_2O were used as precursor and oxidant gas, respectively, and the growth temperature was 300 °C. The Al_2O_3/GaN samples were annealed up to 900 °C for 5 min in a N_2 atmosphere.

For measurements of the electrical properties, a Pt(100 nm) layer was deposited on the ALD-Al_2O_3 film through a shadow mask to provide gate contacts and Pt(100 nm)/Ti(20 nm) ohmic contacts were deposited on the GaN substrate. The *C*–*V* characteristics were measured at a frequency of 1 MHz using an Agilent B1500A semiconductor device parameter analyzer. The flat-band voltage V_{fb} was estimated from the *C*–*V* data using a simulation program.[31] The current-voltage (*I*–*V*) measurement was performed using a Keithley 4200-SCS semiconductor characterization system. The measurements were done in darkness and under illumination with a semiconductor laser (wavelength = 375 nm). Photoluminescence (PL) spectra of the Al_2O_3/GaN samples were measured by using a 325-nm He-Cd laser as an excitation source and a Princeton Instruments SP-300i monochromater. All measurements were performed at room temperature.

Details on the positron annihilation technique are described elsewhere.[22,23,32,33] In the present experiment, the Doppler broadening spectra of the annihilation radiation were measured using a Ge detector as a function of the incident positron energy E in darkness, while the sample was illuminated with a 325-nm He-Cd laser. The laser beam was defocused at the sample position, and the total area of the sample was illuminated with an irradiance of 10 mW/cm^2. The measured spectra were characterized by the S parameter, defined as the fraction of annihilation events in the energy range of 510.24–511.76 keV. The measured $S(E)$ profiles were analyzed by VEPFIT, a computer program developed by van Veen *et al.*[34] In the analysis, the sample structure was divided into three or four blocks. The *S*–*E* curves were fitted by using

$$S(E) = S_e F_e(E) + S_s F_s(E) + \Sigma S_i F_i(E), \quad (1)$$

where $F_e(E)$ is the fraction of non-thermalized (epithermal) positrons annihilated at the surface and $F_s(E)$ and $F_i(E)$ are the fractions of thermalized positrons annihilated at the surface and in the i-th layer, respectively [$F_e(E) + F_s(E) + \Sigma F_i(E) = 1$]. S_e, S_s, and S_i are S parameters that correspond to the annihilation of epithermal positrons at the surface, that of thermalized positrons at the surface, and that of positrons in the i-th layer, respectively.

The lifetime spectrum of positrons implanted into the Al_2O_3 film was measured by using a pulsed monoenergetic positron beam[35] at the NEPOMUC positron source of the Technische Universität München.[36,37] Approximately 4×10^6 counts were accumulated for a lifetime spectrum. The spectrum $S_{LT}(t)$ is given by $S_{LT}(t) = \Sigma\ (1/\tau_i)\ I_i \exp(-t/\tau_i)$, where τ_i and I_i are the positron lifetime and the intensity of the i-th component, respectively ($\Sigma I_i = 1$). The spectra were analyzed with a time resolution of about 200 ps [full-width at half-maximum (FWHM)] by using the RESOLUTION computer program.[38]

Using electron energy loss-spectroscopy, Kimoto *et al.*[39] characterized ALD-Al_2O_3 formed on the Si substrate. They reported that observed energy-loss near edge structures were well explained by assuming Al atoms tetrahedrally and octahedrally coordinated by oxygen (denoted as T_d and O_h sites, respectively), suggesting that the atomic coordinate of ALD-Al_2O_3 is close to that of γ-Al_2O_3. Consequently, in the present work, the positron lifetimes in γ-Al_2O_3 were calculated using the QMAS (Quantum MAterials Simulator) code. Details of the calculation procedure are described elsewhere.[40,41] In a spinel-like γ-Al_2O_3 structure, eight Al vacancies (V_{Al}s) exist in three spinel unit cells to satisfy stoichiometry. Depending on the growth technique or conditions of γ-Al_2O_3, V_{Al}s could locate at both T_d and O_h sites, but the first-principles calculation suggested that V_{Al}s preferentially are located at O_h sites.[42,43]

In the present work, calculations were performed on a monoclinic supercell equivalent to three conventional spinel unit cells.[44] The supercell was constructed as follows. According to Ref. 44, lattice vectors $\mathbf{a} = a_0(0,1/2,1/2)$, $\mathbf{b} = a_0(1/2,0,1/2)$, and $\mathbf{c} = a_0(3/2,3/2,0)$ were constructed, where a_0 represents an experimentally obtained cubic spinel lattice constant (0.7911 nm).[45] Then, a compact unit cell was obtained by changing bases; $\mathbf{a}' = -\mathbf{b}$, $\mathbf{b}' = \mathbf{b} - \mathbf{a}$, and $\mathbf{c}' = \mathbf{a} + \mathbf{b} - \mathbf{c}$. Finally, the supercell with dimensions of $2\mathbf{a}' \times 2\mathbf{b}' \times \mathbf{c}'$ was constructed. In the supercell, the total number of Al sites was 72 and eight Al atoms were removed from the cell using random numbers. The calculations were done for the supercells with V_{Al}s at the O_h site and those with V_{Al} at O_h and T_d sites. Atomic positions in the fixed cell were computationally optimized through a series of first-principles calculations. For each system, we assumed a neutral charge state. The enhancement factor of the positron wave functions used in the calculation was given by $\gamma = 1 + (\gamma_{BN} - 1)\ (1 - 1/\varepsilon_\infty)$, where γ_{BN} is the Boroński-Nieminen enhancement factor.[46] For the high-frequency dielectric constant, ε_∞, we used a value of 3.0 by a reference to ε_∞ of α-Al_2O_3.[47]

III. RESULTS AND DISCUSSION

A. Defects and open spaces in the Al_2O_3/GaN structure

Figure 1 shows the S values of the Al_2O_3(25 nm)/GaN samples before and after annealing at 800 °C and 900 °C. All measurements were performed in darkness. The S value decreased as E increased due to positron annihilation in the GaN template. The S value for positron annihilation in HVPE-GaN was reported to be 0.441 corresponding to positron annihilation in defect-free GaN.[48,49] Using the relationship between the mean implantation depth of positrons and E,[22] the E value corresponding to the thickness of the Al_2O_3 film was calculated to be 2 keV. For the as-deposited sample, therefore, the observed increase in the S value at $E \cong 1$ keV

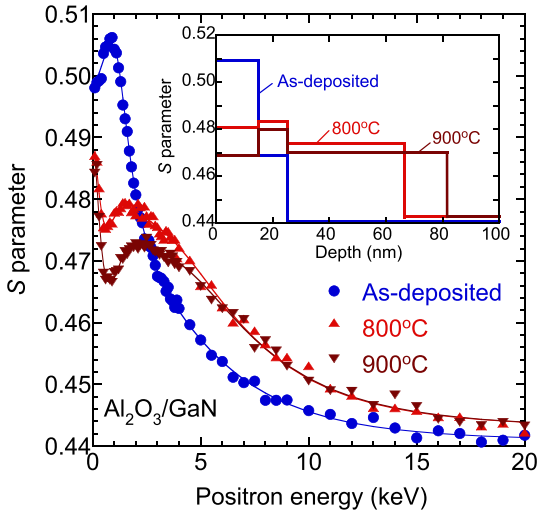

FIG. 1. *S* parameters as a function of incident positron energy *E* for the Al_2O_3(25 nm)/GaN sample before and after annealing treatments (800 °C and 900 °C). Solid curves are fits to experimental data. The inset shows the depth distributions of *S* obtained from fitting.

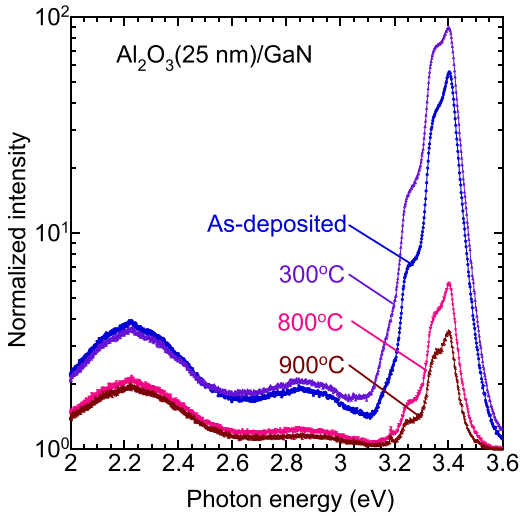

FIG. 2. PL spectra of Al_2O_3(25 nm)/GaN samples before and after annealing. Suppression of PL intensity for samples after annealing at 800 and 900 °C is attributed to the introduction of non-radiative recombination centers in the template.

was associated with the annihilation of positrons in the Al_2O_3 film. The *S* value for a bulk α-Al_2O_3 sample with no-defect response was obtained to be 0.415. The large *S* value at $E \cong 1$ keV, therefore, suggests the annihilation of positrons trapped by open spaces in the amorphous structure. For the annealed samples, the *S* value at $E \cong 1$ keV decreased, but humps appeared at $E = 2$–3 keV, which can be attributed to the introduction of vacancy-type defects below the Al_2O_3/GaN interface.

The obtained *S*–*E* curves were analyzed by using the VEPFIT code, and the solid curves in Fig. 1 were fitted to the experimental data. In the fitting, the region sampled by positrons was divided into three blocks for the as-deposited sample and into four blocks for the annealed samples, respectively. Here, the first and second blocks correspond to the annihilation of positrons in the Al_2O_3 film. The inset of Fig. 1 shows the derived depth distributions of *S* obtained from the fittings. For the annealed samples, the vacancy-type defects were found to be introduced up to a depth of 40–50 nm from the Al_2O_3/GaN interface. For group-III nitride semiconductors, a cation vacancy is the trapping center of positrons, but the N vacancy (V_N) does not trap a positron because of its positive charge.[32,33] Thus, the species of defects causing the increase in *S* can be identified as Ga vacancies (V_{Ga}s) and/or their complexes such as $(V_{Ga})_n(V_N)_m$ (n, m = 1, 2, 3…). The introduction of such vacancies can be attributed to the atomic diffusion from the GaN substrate into the Al_2O_3 film during the annealing treatment.

Figure 2 shows the PL spectra measured for the Al_2O_3/GaN samples before and after annealing at 300, 800, and 900 °C. For the as-deposited sample, the PL spectrum mainly exhibited ultraviolet (3.2–3.6 eV) and yellow luminescence (about 2.2 eV) bands. Ultraviolet luminescence (UVL) corresponds to near band edge (NBE) emission, and the peak broadening on the lower energy side could be due to an incorporation of luminescence originating from excitons bound to defects, donor-acceptor-pair transitions, etc.[50] Yellow luminescence (YL) is typical for GaN containing complexes of vacancies and oxygen or carbon.[50–52] The intensity of the NBE emission increased after temperature treatment at 300 °C, which could be due to the improved crystal quality near the Al_2O_3/GaN interface. However, the *S*–*E* curve for the as-grown sample can be analyzed without assuming the defective region in GaN, suggesting that the introduction of vacancy-type defects was not observed before annealing. After annealing at 800 and 900 °C, both UVL and YL are significantly lower. Because the penetration depth of the He-Cd laser light is estimated to be about 100 nm for GaN, the excitation of electrons mainly occurs just below the Al_2O_3/GaN interface. The observed decrease in PL intensities, therefore, can be attributed to non-radiative recombination centers introduced near the Al_2O_3/GaN interface.

Figure 3 shows the annealing behavior of (a) the intensity of NBE, (b) V_{fb} derived from the *C*–*V* measurements, and (c) the *S* values for the Al_2O_3/GaN samples. The *S* values at $E = 0.8$ and 2.2 keV correspond to the annihilation of positrons in the Al_2O_3 film and in the GaN template just below the Al_2O_3/GaN interface, respectively. To increase statistical accuracy, those *S* values were averaged by using the values measured at $E = 0.7$–0.9 and 2.0–2.4 keV, respectively. The statistical error of the *S* value is 5×10^{-4}, and the corresponding error bars are smaller than the size of symbol used in the figure. At 800 °C annealing, the decrease in *S* at $E = 0.8$ keV suggests that the size of open spaces decreased in the Al_2O_3 film. At this temperature, because the suppression of PL was observed, the defects introduced below the Al_2O_3/GaN interface (inset of Fig. 1) were likely to act as non-radiative recombination centers.

Figure 3(b) shows the annealing behavior of V_{fb} measured in darkness and under illumination. An ideal V_{fb} for the gate stack used in the present work was calculated to be 1 V. For the as-deposited sample, a negative V_{fb} value was observed. A similar behavior of V_{fb} for Al_2O_3/GaN stacks was often reported, and this was attributed to the presence of

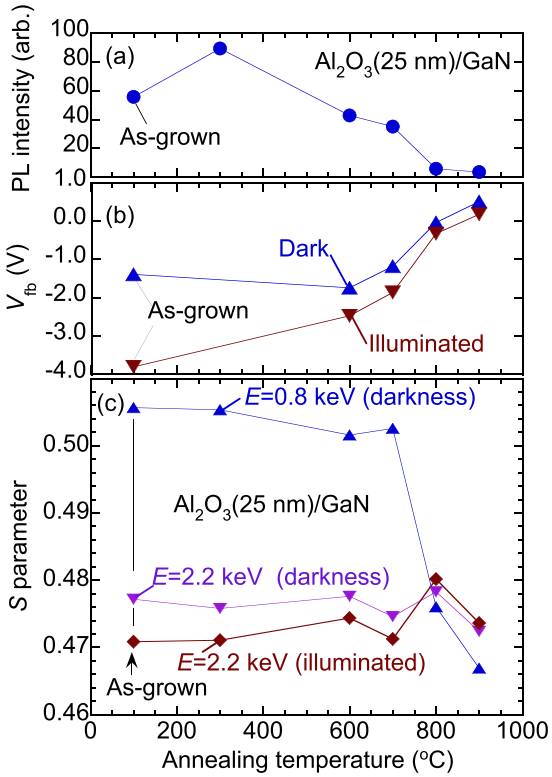

FIG. 3. (a) PL intensity corresponding to NBE, (b) V_{fb}, and (c) S measured at $E = 0.8$ and 2.2 keV before and after annealing. Values of V_{fb} and S at $E = 2.2$ keV were measured both in darkness and under illumination, respectively.

positive charges fixed at the interface.[16,19,20] The V_{fb} value increased as the annealing temperature increased, suggesting that the density of net positive charges decreased due to annealing up to 900 °C. Under illumination, the value of V_{fb} decreased, but the difference between the values measured with and without illumination decreased as the annealing temperature increased. We will come back to this point later.

Figure 4 shows the relationship between the current density J and the electric field E_{eff} applied in the template for the Al_2O_3(25 nm)/GaN sample before and after annealing treatments (600–900 °C). The leakage of the Al_2O_3/GaN stack was suppressed with increasing annealing temperature up to 700 °C. For the samples annealed at 800 and 900 °C, however, spike-like leakage started to appear. The observed degradation of the leakage current blocking capability is considered to relate to the change in the amorphous structure of the Al_2O_3 film after annealing above 800 °C.

For the samples before and after annealing at 800 and 900 °C, the lifetime spectra of positrons were measured at $E = 1$ keV, which correspond to the annihilation of positrons in the Al_2O_3 film. The lifetime spectra were decomposed into three components, and the obtained lifetimes with corresponding intensities are shown in Fig. 5. Standard deviations of these parameters are smaller than the size of symbols used in the figure. The third lifetime (τ_3) is typical for the annihilation of positronium (Ps: a hydrogen-like bound state between a positron and an electron). When a positron is trapped by an open space, it could couple with an electron and form Ps. Ps exhibits two spin states: para-Ps (p-Ps), a

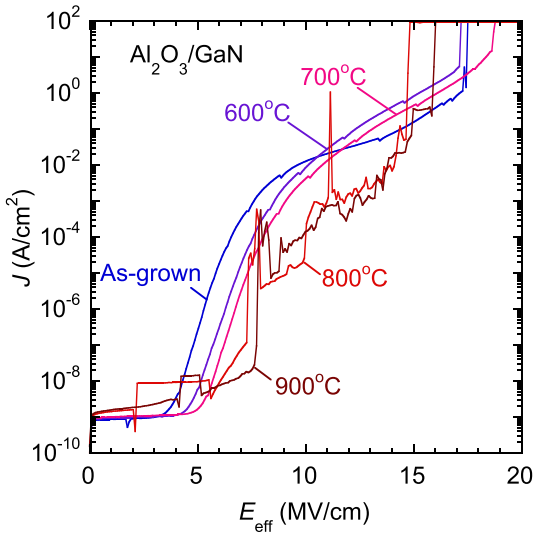

FIG. 4. Current density J and electric field E_{eff} applied in the template for the Al_2O_3(25 nm)/GaN sample before and after annealing treatments (600–900 °C).

singlet state, and ortho-Ps (o-Ps), a triplet state.[53] The intrinsic vacuum lifetimes of p-Ps and o-Ps are 125 ps and 142 ns, respectively. P-Ps annihilates via the 2-γ process, and the energy of the emitted γ-rays is 511 keV. Thus, the value of S is sensitive to the formation probability of Ps. When o-Ps is trapped in a void, the positron may annihilate with a surrounding electron of opposite spin, resulting in the emission of two γ-rays instead of 3γ-annihilation. A large open space reduces the probability of this so-called pick-off process and increases the o-Ps lifetime. According to the relationship between the o-Ps lifetime and the void size used for amorphous polymers,[53] the diameter of the voids (which are assumed to be spherical) in the as-deposited and annealed samples can be estimated to be 0.6 and 0.9 nm, respectively.

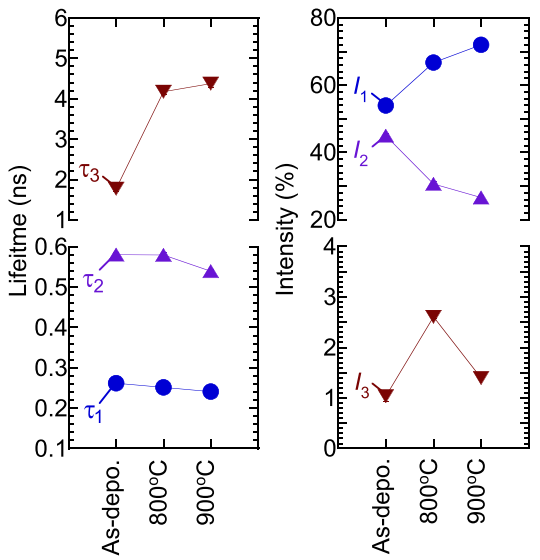

FIG. 5. (a) Positron lifetimes (τ_1, τ_2, and τ_3) and (b) their intensities (I_1, I_2, and I_3) measured at $E = 1$ keV for Al_2O_3/GaN samples before and after annealing. In this energy range, almost all positrons annihilate in the Al_2O_3 film. The values of τ_1, τ_2, and I_2 decrease as annealing temperature increases, suggesting that the matrix structure of the Al_2O_3 film shrunk.

Because the I_3 values are 1%–3%, however, they are not the major open spaces in the Al_2O_3 film.

The lifetime of positrons annihilated from the free state in crystalline α-Al_2O_3 was 143 ps.[54] Because the first and second positron lifetimes (τ_1 and τ_2) were longer than this value (Fig. 5), they are associated with the annihilation of positrons trapped by open spaces. The intrinsic lifetime of *p*-Ps (0.125 ns) is likely to be involved in the τ_1 value, but its effect is small (because of a small I_3). Thus, one can conclude that open spaces with three different sizes coexisted in the as-deposited Al_2O_3 film, and this is also true for the film annealed up to 900 °C. As shown in Fig. 5, the values of τ_1, τ_2, and I_2 decreased as the annealing temperature increased, suggesting that the amorphous structure shrunk and the open spaces and their density decreased as well.

Figures 6(a) and 6(b) show an example of atomic configurations of γ-Al_2O_3 used in the calculation and a corresponding distribution of the positron density, respectively. Light blue, red, and black circles correspond to Al, O, and V_{Al}, respectively. Figures 6(c) and 6(d) show another set of atomic configuration and positron density distribution. For the supercell shown in Figs. 6(a) and 6(c), the positron lifetimes were obtained to be 0.220 ns and 0.245 ns, respectively. In Fig. 6(c), three V_{Al}s locate near the center of the supercell. This caused the localization of positrons at the center, and the large open space increased the positron lifetime. In Fig. 6(b), the positrons of V_{Al}s were rather scattered, shortening the positron lifetime.

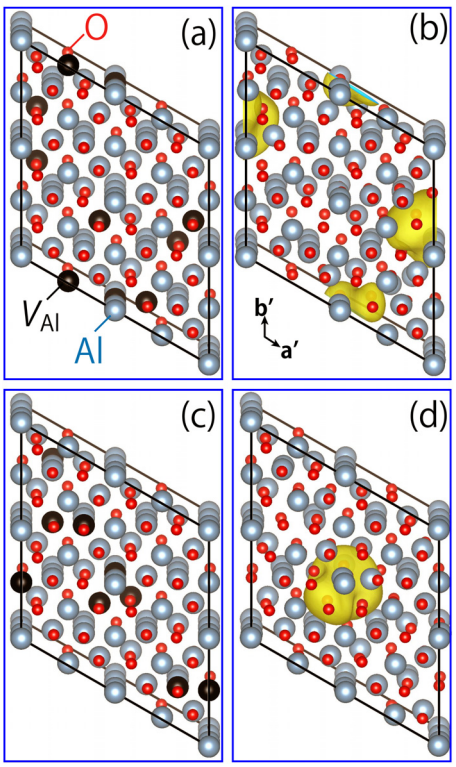

FIG. 6. Examples of atomic configurations of γ-Al_2O_3 used in the calculation [(a) and (c)] and corresponding distributions of the positron densities [(b) and (d)]. Light blue, red, and black circles correspond to Al, O, and V_{Al}, respectively. The positions of eight vacant Al sites in the supercell were determined using random numbers.

Figure 7 shows the frequency distributions of the calculated positron lifetimes for γ-Al_2O_3. The mean positron lifetime was obtained to be 0.242 ns. Because this value is close to τ_1 shown in Fig. 5, the first annihilation mode can be attributed to the positron annihilation in the atomic structure close to that of γ-Al_2O_3. The τ_1 value decreased from 0.26 ns to 0.24 ns with increasing annealing temperature. According to the simulation results shown in Fig. 6, annealing could cause the dissociation of V_{Al} clusters.

B. Effects of illumination on GaN and Al_2O_3/GaN stacks

Figure 8 shows the *S*–*E* curves for the GaN template measured in darkness and with illumination. The mean implantation depth of positrons is shown on the upper horizontal axis. The *S* value increased as *E* decreased, which corresponds to the diffusion of positrons toward the surface. From the fitting of the *S*–*E* curve for the sample measured in darkness, the diffusion length of positrons toward the surface L_d was derived as 59 ± 1 nm. The *S*–*E* curve measured with illumination can be fitted by using the value of L_d obtained for the result measured in darkness. A major origin that causes a difference in *S*–*E* curves with and without illumination is the differences in the values of S_s, which were obtained to be 0.4715 ± 0.004 and 0.4432 ± 0.004 for the sample without and with illumination, respectively. For bulk GaN grown by supercritical acidic ammonothermal technology, a similar illumination effect on the *S*–*E* curve was reported previously, and the details on what causes the decrease in the *S* value are given in Ref. 48.

The inset of Fig. 8 shows a schematic band diagram of an *n*-type semiconductor under illumination, where E_V and E_C are the energies of the valence-band maximum and the conduction-band minimum, respectively.[55] A circle and a square represent an electron and a hole, respectively. The electric field caused by upward band bending causes

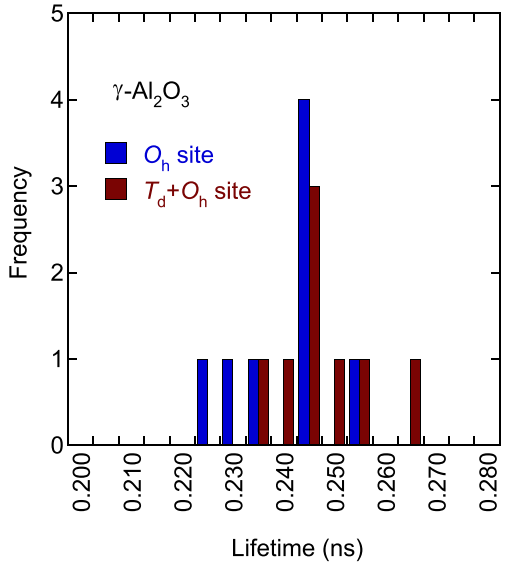

FIG. 7. Frequency distributions of the calculated positron lifetimes for γ-Al_2O_3. The positron lifetimes were calculated for supercells with V_{Al} at the O_h site and for ones with V_{Al} at the T_d and O_h sites, respectively.

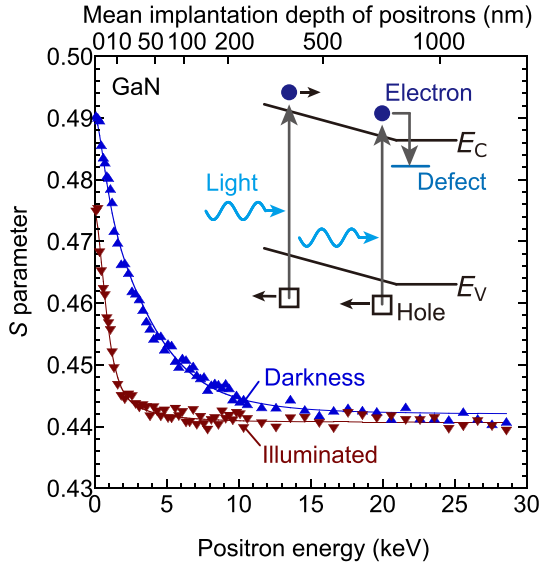

FIG. 8. *S*–*E* curves for the GaN template measured in darkness and under illumination. The inset shows the schematic band diagram for *n*-type semiconductors under illumination.

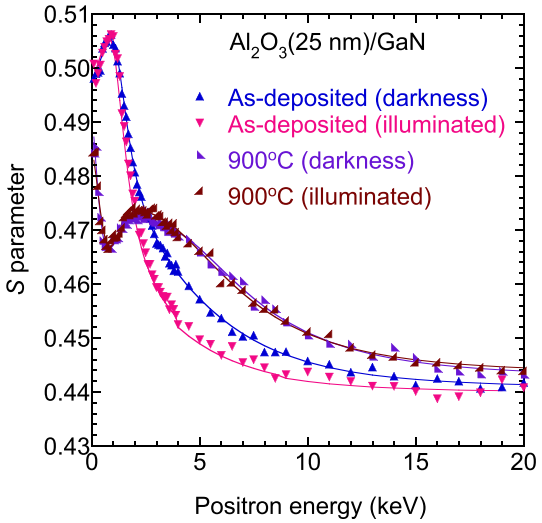

FIG. 9. *S*–*E* curves for as-deposited and tempered Al_2O_3 (25 nm)/GaN samples measured in darkness and under illumination. For the as-deposited sample with illumination, the decrease in the *S* value at $E > 1$ keV is attributed to excitation of electron traps at the Al_2O_3/GaN interface.

electrons excited from the valence band to the conduction band to be swept away from the surface and holes to diffuse to the surface. For semiconductors, S_s is larger than S_b because of the formation of Ps and the positron annihilation with electrons at the surface. The positron wave function at the surface could be pushed back toward the bulk by the presence of holes at the surface, and this would suppress the positron-electron annihilation and the Ps annihilation at the surface. As a result, the S_s value is decreased by illumination.

For the GaN template used in the present experiment, the recovery of the S_s value required almost one day. This fact suggests that the decrease in the S_s value under illumination was caused by the hole accumulation at the surface due to the suppression of the electron-hole recombination. Electrons excited by illumination are considered to be captured by traps, which can hold electrons for a long time. Because the bulk *S* value for the GaN template was close to the defect free value, the electron traps were likely to be non-vacancy defects or vacancies which are not detectable by positron annihilation (such as V_N).

Figure 9 shows the *S*–*E* curves for the Al_2O_3(25 nm)/GaN samples without and with illumination. For the as-deposited sample, the *S* value at $E > 1$ keV was decreased by illumination, which is similar to the result observed for the GaN template (Fig. 8). The decrease in *S* can be attributed to the positive charges near the Al_2O_3/GaN interface introduced by illumination. Figure 10 shows the schematic band diagrams of the samples before and after annealing. Because the V_{fb} value was negative for the as-deposited sample [Fig. 3(b)], a certain amount of positive charge was located at the interface [Fig. 10(a)]. As shown in Fig. 3(b), the value of V_{fb} decreased under illumination, which suggests that neutral traps were excited at the interface. As discussed above, the excess electrons could be captured by the defects in the GaN template (inset of Fig. 8). As a result, positive charges accumulated at the interface [Fig. 10(b)] and prevent the diffusion of positrons toward the Al_2O_3 film. Because the *S* value in the Al_2O_3 film was larger than that in GaN, the decrease in the annihilation probability of positrons in the Al_2O_3 film decreased the *S* value.

Figure 3(c) shows the annealing behavior of *S* measured at $E = 2.2$ keV for the samples with and without illumination. The *S* values for the samples before and after annealing below 700 °C were decreased by illumination, which is due to the introduction of positive charges at the interface. Above 800 °C, however, the *S* values increased under illumination, where the statistical error of the *S* value is smaller than the size of the symbol used in the figure. An increase in the *S* value measured under illumination was reported for the GaN film grown on Si[56,57] and ion-implanted GaN.[58] Since positrons are attracted or repelled by vacancy-type defects through Coulomb forces, the transition of the charge state of vacancies (*V*) from positive to neutral (or neutral to negative), $V^+ \rightarrow V^0$ (or $V^0 \rightarrow V^-$), increases the positron trapping probability.[22] Thus, the observed increase in the *S* value can be attributed to the capture of photon-excited electrons

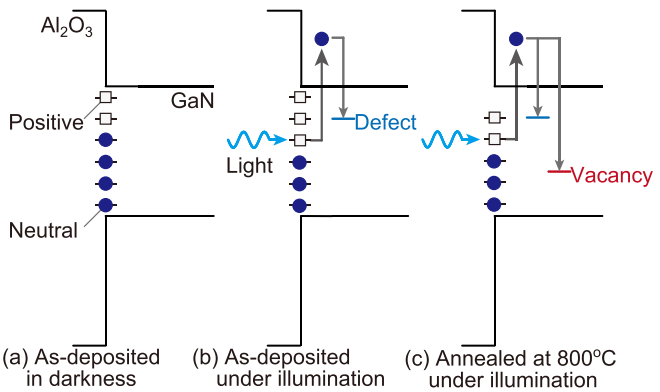

FIG. 10. Schematic band diagrams of as-deposited Al_2O_3/GaN samples in darkness (a) and under illumination (b). (b) Neutral traps are excited under illumination and emitted electrons are captured by traps in the GaN template. (c) Capture of electrons by vacancy-type defects introduced by outdiffusion of atoms.

by vacancy-type defects and the resultant charge transition of the defects. This fact suggests that the vacancy-type defects introduced by the reaction between the Al_2O_3 film and GaN acted as electron trapping centers [Fig. 10(c)].

IV. SUMMARY

We used monoenergetic positron beams to probe vacancy-type defects in the Al_2O_3/GaN structure. Al_2O_3 films were deposited on GaN templates by using the ALD technique. Doppler broadening spectra were measured as a function of incident positron energy for samples before and after annealing (300–900 °C). After annealing at 800 °C, vacancy-type defects were introduced into the GaN template because of the outdiffusion of atoms from the template into the Al_2O_3 film. The width of the defect-rich region was 40–50 nm from the Al_2O_3/GaN interface. From positron lifetime measurements of the as-deposited Al_2O_3 film, open spaces with three different sizes were found to coexist in the film. After annealing at 800 °C, the density of the medium-sized open spaces decreases, which correlates with the interaction between the GaN template and the Al_2O_3 film.

The density of positive charges at the Al_2O_3/GaN interface decreased as the annealing temperature increases up to 900 °C. The positive charge densities at the interface increases under illumination due to the excitation of neutral traps at the interface. For the samples before and after annealing below 700 °C, the electrons excited from the interface traps localize around defects in the GaN template, and as a result, hole accumulation occurs at the interface. The present research suggests that the interaction between amorphous Al_2O_3 and GaN not only introduces vacancy-type defects in GaN but also changes the matrix structure of the Al_2O_3 film. We also revealed that the electron trapping/detrapping processes of interface charge states are influenced by the defects introduced in GaN.

ACKNOWLEDGMENTS

This work was supported by the MEXT "Program for research and development of next-generation semiconductor to realize energy-saving society." A part of this work was also supported by JSPS KAKENHI (Grant No. 16H06424) and the Cross-ministerial Strategic Innovation Promotion Program (SIP), "Next-generation power electronics" (funding agency: NEDO).

[1]U. K. Mishra, L. Shen, T. E. Kazior, and Y.-F. Wu, Prof. IEEE **96**, 287 (2008).
[2]B. J. Baliga, Semicond. Sci. Technol. **28**, 074011 (2013).
[3]M. A. Khan, M. S. Shur, J. N. Kuznia, Q. Chen, J. Burm, and W. Schaff, Appl. Phys. Lett. **66**, 1083 (1995).
[4]O. Aktas, Z. F. Fan, S. N. Mohammad, A. E. Bothkarev, and H. Morkoc, Appl. Phys. Lett. **69**, 3872 (1996).
[5]N. Maeda, T. Saitoh, K. Ttsubaki, T. Nishida, and N. Kobayashi, Jpn. J. Appl. Phys., Part 2 **38**, L987 (1999).
[6]Y. Nakano, T. Kachi, and T. Jimbo, J. Vac. Sci. Technol., B **21**, 2220 (2003).
[7]Y. Zhou, C. Ahyi, T. Issacs-Smith, M. Bozack, C.-C. Tin, J. Williams, M. Park, A.-J. Cheng, J.-H. Park, D.-J. Kim, D. Wang, E. A. Preble, A. Hanser, and K. Evans, Solid-State Electron. **52**, 756 (2008).
[8]M. Grodzicki, P. Mazur, S. Zuber, J. Brona, and A. Ciszewski, Appl. Surf. Sci. **304**, 20 (2014).
[9]T. Yamada, J. Ito, R. Asahara, K. Watanabe, M. Nozaki, S. Nakazawa, Y. Anda, M. Ishida, T. Ueda, A. Yoshigoe, T. Hosoi, T. Shimura, and H. Watanabe, J. Appl. Phys. **121**, 035303 (2017).
[10]M. A. Kahn, X. Hu, A. Tarakji, G. Simin, J. Yang, R. Gaska, and M. S. Sher, Appl. Phys. Lett. **77**, 1339 (2000).
[11]N. Maeda, C. Wang, T. Enoki, T. Makimoto, and T. Tawara, Appl. Phys. Lett. **87**, 073504 (2005).
[12]T. Hashizume, S. Ootomo, S. Oyama, M. Konishi, and H. Hasegawa, J. Vac. Sci. Technol., B **19**, 1675 (2001).
[13]X. Hu, A. Koudymov, G. Simon, J. Yang, M. Asif Khan, A. Tarakji, M. S. Shur, and R. Gaska, Appl. Phys. Lett. **79**, 2832 (2001).
[14]S. Huang, S. Yang, J. Roberts, and K. J. Chen, Jpn. J. Appl. Phys. **50**, 110202 (2011).
[15]Y. Hori, C. Mizue, and T. Hashizume, Jpn. J. Appl. Phys., Part 1 **49**, 080201 (2010).
[16]X. Qin and R. M. Wallace, Appl. Phys. Lett. **107**, 081608 (2015).
[17]R. Asahara, M. Nozaki, T. Yamada, J. Ito, S. Nakazawa, M. Ishida, T. Ueda, A. Yoshigoe, T. Hosoi, T. Shimura, and H. Watanabe, Appl. Phys. Express **9**, 101002 (2016).
[18]M. Matys, B. Adamowicz, A. Domanowska, A. Michalewicz, R. Stoklas, M. Akazawa, Z. Yatabe, and T. Hashizume, J. Appl. Phys. **120**, 225305 (2016).
[19]M. Matys, R. Stoklas, M. Blaho, and B. Adamowicz, Appl. Phys. Lett. **110**, 243505 (2017).
[20]K. Watanabe, M. Nozaki, T. Yamada, S. Nakazawa, Y. Anda, M. Ishida, T. Ueda, A. Yoshigoe, T. Hosoi, T. Shimura, and H. Watanabe, Appl. Phys. Lett. **111**, 042102 (2017).
[21]J. Robertson, Eur. Phys. J. Appl. Phys. **28**, 265 (2004).
[22]R. Krause-Rehberg and H. S. Leipner, *Positron Annihilation in Semiconductors, Solid-State Sciences* (Springer-Verlag, Berlin, 1999), Vol. 127.
[23]F. Tuomisto and I. Makkonen, Rev. Mod. Phys. **85**, 1583 (2013).
[24]K. Saarinen, T. Laine, S. Kuisma, J. Nissilä, P. Hautojärvi, L. Dobrzynski, J. M. Baranowski, K. Pakula, R. Stepniewski, M. Wojdak, A. Wysmolek, T. Suski, M. Leszczynski, I. Grzegory, and S. Porowski, Phys. Rev. Lett. **79**, 3030 (1997).
[25]K. Saarinen, T. Suski, I. Grzegory, and D. C. Look, Phys. Rev. B **64**, 233201 (2001).
[26]A. Uedono, S. F. Chichibu, Z. Q. Chen, M. Sumiya, R. Suzuki, T. Ohdaira, T. Mikado, T. Mukai, and S. Nakamura, J. Appl. Phys. **90**, 181 (2001).
[27]J. Oila, J. Kivioja, V. Ranki, K. Saarinen, D. C. Look, R. J. Molnar, S. S. Park, S. K. Lee, and J. Y. Han, Appl. Phys. Lett. **82**, 3433 (2003).
[28]A. Uedono, T. Naito, T. Otsuka, K. Shiraishi, K. Yamabe, S. Miyazaki, H. Watanabe, N. Umezawa, T. Chikyow, Y. Akasaka, S. Kamiyama, Y. Nara, and K. Yamada, J. Appl. Phys. **100**, 064501 (2006).
[29]A. Uedono, K. Ikeuchi, T. Otsuka, K. Shiraishi, S. Miyazaki, N. Umezawa, A. Hamid, T. Chikyow, T. Ohdaira, M. Muramatsu, R. Suzuki, S. Inumiya, S. Kamiyama, Y. Akasaka, Y. Nara, and K. Yamada, J. Appl. Phys. **99**, 054507 (2006).
[30]Y. Irokawa, T. T. Suzuki, K. Yuge, A. Ohi, T. Nabatame, K. Kimoto, T. Ohnishi, K. Mitsuishi, and Y. Koide, Jpn. J. Appl. Phys., Part 1 **56**, 128004 (2017).
[31]T. Nabatame, A. Ohi, T. Chikyo, M. Kimura, H. Yamada, and T. Ohishi, J. Vac. Sci. Technol., B **32**, 03D121 (2014).
[32]A. Uedono, S. Ishibashi, N. Oshima, and R. Suzuki, Jpn. J. Appl. Phys., Part 1 **52**, 08JJ02 (2013).
[33]A. Uedono, S. Takashima, M. Edo, K. Ueno, H. Matsuyama, H. Kudo, H. Naramoto, and S. Ishibashi, Phys. Status Solidi B **252**, 2794 (2015).
[34]A. van Veen, H. Schut, M. Clement, J. M. M. de Nijs, A. Kruseman, and M. R. IJpma, Appl. Surf. Sci. **85**, 216 (1995).
[35]P. Sperr, W. Egger, G. Kögel, G. Dollinger, C. Hugenschmidt, R. Repper, and C. Piochacz, Appl. Surf. Sci. **255**, 35 (2008).
[36]C. Hugenschmidt, B. Löwe, J. Mayer, C. Piochacz, P. Pikart, R. Repper, M. Stadlbauer, and K. Schreckenbach, Nucl. Instrum. Methods A **593**, 616 (2008).
[37]C. Hugenschmidt, J. Phys.: Conf. Ser. **262**, 012002 (2011).
[38]P. Kirkegaard, M. Eldrup, O. E. Mogensen, and N. J. Pedersen, Comput. Phys. Commun. **23**, 307 (1981).
[39]K. Kimoto, Y. Matsui, T. Nabatame, T. Yasuda, T. Mizoguchi, I. Tanaka, and A. Toriumi, Appl. Phys. Lett. **83**, 4306 (2003).
[40]S. Ishibashi, T. Tamura, S. Tanaka, M. Kohyama, and K. Terakura, Phys. Rev. B **76**, 153310 (2007).
[41]S. Ishibashi and A. Uedono, J. Phys. Conf. **505**, 012010 (2014).

[42]F. H. Streitz and J. W. Mintmire, Phys. Rev. B **60**, 773 (1999).
[43]C. Y. Ouyang, Ž. Šljivančanin, and A. Baldereschi, Phys. Rev. B **79**, 235410 (2009).
[44]E. Menéndez-Proupin and G. Gutiérrez, Phys. Rev. B **72**, 035116 (2005).
[45]R.-S. Zhou and R. L. Snyder, Acta Crystallogr., Sect. B **47**, 617 (1991).
[46]E. Boroński and R. M. Nieminen, Phys. Rev. B **34**, 3820 (1986).
[47]A. K. Harman, S. Ninomiya, and S. Adachi, J. Appl. Phys. **76**, 8032 (1994).
[48]A. Uedono, Y. Tsukada, Y. Mikawa, T. Mochizuki, H. Fujisawa, H. Ikeda, K. Kurihara, K. Fujito, S. Terada, S. Ishibashi, and S. F. Chichibu, J. Cryst. Growth **448**, 117 (2016).
[49]A. Uedono, M. Imanishi, M. Imade, M. Yoshimura, S. Ishibashi, M. Sumiya, and Y. Mori, J. Cryst. Growth **475**, 261 (2017).
[50]M. A. Reshchikova and H. Morkoç, J. Appl. Phys. **97**, 061301 (2005).
[51]J. L. Lyons, A. Janotti, and C. G. Van de Walle, Appl. Phys. Lett. **97**, 152108 (2010).
[52]M. A. Reshchikov, D. O. Demchenko, A. Usikov, H. Helava, and Yu. Makarov, Phys. Rev. B **90**, 235203 (2014).
[53]*Principle and Application of Positron and Positronium Chemistry*, edited by Y. C. Jean and D. M. Schrader (World Scientific, Singapore, 2003), p. 167.
[54]A. Uedono, K. Ikeuchi, K. Yamabe, T. Ohdaira, M. Muramatsu, R. Suzuki, A. S. Hamid, T. Chikyow, K. Torii, and K. Yamada, J. Appl. Phys. **98**, 023506 (2005).
[55]L. Kronik and Y. Shapir, Surf. Interface Anal. **31**, 954 (2001).
[56]A. Uedono, T. Fujishima, D. Piedra, N. Yoshihara, S. Ishibashi, M. Sumiya, O. Laboutin, W. Johnson, and T. Palacios, Appl. Phys. Lett. **105**, 052108 (2014).
[57]A. Uedono, T. Tanaka, N. Ito, K. Nakahara, W. Egger, C. Hugenschmidt, S. Ishibashi, and M. Sumiya, Thin Solid Films **639**, 78 (2017).
[58]A. Uedono, S. Takashima, M. Edo, K. Ueno, H. Matsuyama, W. Egger, T. Koschine, C. Hugenschmidt, M. Dickmann, K. Kojima, S. F. Chichibu, and S. Ishibashi, Phys. Status Solidi B **2017**, 1700521.